The Variability of Relationship between Black Carbon and Carbon Monoxide over the Eastern Coast of China: BC Aging during Transport

Qingfeng Guo[1], Min Hu[1,2], Song Guo[1], Zhijun Wu[1], Jianfei Peng[1], Yusheng Wu[1]

[1]State Key Joint Laboratory of Environmental Simulation and Pollution Control, College of Environmental Sciences and Engineering, Peking University, Beijing 100871, China
[2]Beijing Innovation Center for Engineering Science and Advanced Technology, Peking University

Correspondence to: Min Hu (minhu@pku.edu.cn)

Abstract. East Asia is a densely populated region with a myriad of primary emissions of pollutants such as black carbon (BC) and carbon monoxide (CO). To characterize primary emissions over the eastern coast of China, a cascade of field campaign was conducted in 2011, including the measurement of ship cruise, island, and coastal receptor sites. The relationship between BC and CO is presented here for the first ship cruise (C1), the second ship cruise (C2), an island site (Changdao Island, CD), and a coastal site (Wenling, WL). The average BC mass concentrations are 2.43, 2.73, 1.09, 0.94, and 0.77 µg·m^{-3} for CD, WL, C1-YS (Yellow Sea), C1-ES (East China Sea), and C2-ES, respectively. For those locations, the average CO mixing ratios are 0.55, 0.48, 0.31, 0.36, and 0.27 ppm. The high loadings of both BC and CO imply the severe anthropogenic pollution over the eastern coast of China. Additionally, the linear correlation between BC and CO is regressed for each location. The slopes, i.e. ΔBC/ΔCO ratios derived from their relationships are correlated well with the ratios of diesel consumption to gasoline consumption in each province/city, which reveals the vehicular emission as the common source for BC and CO and the distinct fuel structures between North and South China. The ΔBC/ΔCO ratios at coastal sites (Changdao Island and Wenling) are much higher than those over Yellow Sea and East China Sea, and the correlation coefficients also show a decreasing trend from the coast to the sea. Therefore, the ΔBC/ΔCO ratio and correlation coefficient are possible indicators for the aging and removal of BC.

1 Introduction

The atmospheric radiative forcing is caused by a variety of particulate and gaseous air pollutants. Among these particulate matters, BC impacts the Earth's climate directly through the absorption of the solar radiation and indirectly through its role as cloud condensation nuclei (Bond et al., 2013). The absorption induced by BC is markedly enhanced by the atmospheric oxidation and aging, as investigated by many chamber studies (Peng et al., 2016;Guo et al., 2016;Schnaiter et al., 2005). Among these gaseous pollutants, CO is an indirect greenhouse gas through the production of ozone, methane, and carbon dioxide (Girach et al., 2014). Both of them are products of incomplete combustion of carbon-based fuels (Wang et al., 2015).

Though BC and CO are from similar sources, their emission ratios vary significantly for different sources, so the variations in measured ratios can indicate the presence of different sources (McMeeking et al., 2010;Bond et al., 2004). The source-specific emission ratio is an important constraint on global climate and regional air quality model (Spackman et al., 2008).

Sources of BC colocated with CO will result in their concentration correlations, since the variances in the concentrations are affected by the same atmospheric process (Wang et al., 2011). There have been a number of studies about the relationship between BC and CO, and they show a remarkable correlation in most studies (e.g. Zhou et al., 2009;Spackman et al., 2008). They have generally been conducted at a stationary site or a cruise, while the simultaneous measurement of the both is rare. The slopes, i.e. $\Delta BC/\Delta CO$ ratios, from the linear regressions are used to indicate different emission sources (Girach et al., 2014;Lee et al., 2013;Pan et al., 2011) and validate BC emissions from the bottom-up inventories (Wang et al., 2011;Han et al., 2009).

For BC, its atmospheric lifecycle includes emissions, transport, aging, and removal (Bond et al., 2013). The relationship between BC and CO is the result of a balance between emission sources and sinks (Spackman et al., 2008;Wang et al., 2015). Thus, differences in emission sources and removal rates (i.e. sinks) are often used to explain differences in $\Delta BC/\Delta CO$ ratios (McMeeking et al., 2010). To a certain extent, the variability due to emissions and transport can be accounted for in $\Delta BC/\Delta CO$ ratio (De Gouw and Jimenez, 2009). The atmospheric lifetime of BC is shorter than CO owing to cloud and precipitation scavenging, which results in the decreasing $\Delta BC/\Delta CO$ with increasing time and distance from source. Therefore, the variations in $\Delta BC/\Delta CO$ ratios also reflect air mass aging and wet removal processes in addition to sources (McMeeking et al., 2010).

Eastern coastal areas are the most developed in China, and are in the transport pathway of the Asian pollution outflow, especially during the East Asia monsoon in winter. The air pollutants emitted from this region and its upwind regions not only result in the deterioration of the air quality on a regional scale, but also exert an influence on downwind countries in the Pacific Rim (Feng et al., 2007;Peltier et al., 2008). In order to characterize the outflow of primary emission over the eastern coast of China, the campaigns including two cruises and two coastal sites were conducted in 2011. Among these, there was a campaign from March to April containing both the island stationary and marine cruise observation.

2 Measurement and Meteorology

2.1 Sampling sites and measurement

To characterize the outflow of the primary emission from East China, four campaigns were conducted in the coastal regions in 2011 (Figure 1). The first one was at Changdao Island (CD, 120.74°E, 37.92°N), Shandong province in north China from 20 March to 24 April, along with the first cruise observation (C1) conducted in Yellow Sea (C1-YS) and East China Sea (C1-ES) from 17 March to 9 April. The second one was the other cruise observation in East China Sea (C2-ES) from 28 May

to 8 June. The third one was at Wenling coastal site (WL, 121.74°E, 28.43°N), Zhejiang province in south China from 1 to 28 November.

As shown in figure 1, Changdao Island (CD) is located off the eastern coast in North China. To its west and south are the cities of Beijing and Tianjin and the provinces of Hebei and Shandong, which have the largest emission of BC in North

5 China. The more detailed description about this site can be seen in the previous studies (Guo et al., 2015;Yuan et al., 2013;Hu et al., 2013). Wenling (WL) is located at the eastern coast in South China. There are a lot of BC emitting at the boundary areas among Yangtz River Delta of Zhejiang, Jiangsu, and Shanghai, which will pose an impact on Wenling when the northwesterly wind is predominant. To the east of Changdao Island and Wenling is Yellow Sea and East China Sea, which are the marginal seas surrounded by China, Korea, and Japan.

10 A suite of online instrument was deployed for gaseous and particulate pollutants measurements during the campaigns. For the primary emission and BC aging are the focuses, both BC and CO hourly averaged data are adopted in this work. BC mass concentrations were continually measured by an optical attenuation technique based Aethalometer (AE-31, Magee Scientific, USA) with an integration time of 5 min. Aethalometer has been widely used for BC measurement and shown excellent agreement with other techniques such as thermal and photo-acoustic (Zhou et al., 2009;Girach et al., 2014;Nair et

15 al., 2007;Hitzenberger et al., 2006). The uncertainty for BC mass concentration was estimated to be 10%. CO mixing ratios were measured by CO analyzer trace level enhacnced (48i-TLE, Thermo Scientific, USA) with an integration time of 1 min. The CO analyzer was calibrated using CO standard every week, and the zero checks were performed every day. The overall uncertainty for CO measurement was estimated to be less than 10%.

2.2 Meteorological conditions

20 Figure 2a - 2d show the mean synoptic wind flow patterns at 925 hPa for Changdao Island (CD), the first cruise (C1), the second cruise (C2), and Wenling (WL) campaign periods, respectively, as obtained from NCEP/NCAR reanalysis (http://www.esrl.noaa.gov/psd). These flow patterns reveal the typical impact of East Asia monsoon over the eastern coast of China, which includes winter and summer monsoon. Generally, the winter monsoon lasts from November to the following April with the prevailing northwestern wind, while the summer monsoon continues from May to October with the

25 predominant southwestern wind.

As can be seen in figure 2a, 2b and 2d, Changdao Island, Yellow Sea and East China Sea, and Wenling are influenced by the winter monsoon during CD, C1, and WL campaign, respectively, whereas East China Sea during C2 (figure 2c) is impacted by the summer monsoon. Though CD and C1 are in the same period, C1 ends two weeks earlier than CD, as the date indicates in figure 1. Consequently, though there is somewhat difference in the wind speed, their flow patterns are basically

30 consistent. In addition, the wind flow pattern during C1 is also comparable with that during WL. However, there is a little discrepancy in the wind direction, which implies that they are in the opposite phases of the winter monsoon, that is, the period during C1 is at the end of the winter monsoon, which will get weaker and transit to the summer monsoon and the

period during WL is at the start of the winter monsoon. The wind flow patterns during the first and second cruise are almost opposite in the wind direction (figure 2b and 2c), which suggests that the air mass during the first cruise mainly flowed from North China to Yellow Sea, and then to East China Sea, whereas during the second cruise, the air mass direction was from South China to East China Sea.

3 Results and Discussion

3.1 Variability of BC and CO concentration

The average BC mass concentrations are 2.43, 1.09, 0.94, 0.77, and 2.73 $\mu g \cdot m^{-3}$ for CD, C1-YS, C1-ES, C2-ES, and WL, respectively. Correspondingly, the average CO mixing ratios are 0.55, 0.31, 0.36, 0.27 and 0.48 ppm. The average concentrations between coastal sites are similar, so are the concentrations between different sea areas. It is no doubt that the pollutants' concentrations at coastal sites are higher than those in the marine atmosphere, but BC and CO in Yellow Sea and East China Sea also have considerable loadings, implying the severe anthropogenic pollution from the continent.

BC and CO at Changdao Island have concentration ranges of 0.3 - 8.5 $\mu g \cdot m^{-3}$ and 0.1 - 2.9 ppm (figure 3a), while BC at Wenling has a wider range of 0.1 - 13.7 $\mu g \cdot m^{-3}$ and CO has a narrower range of 0.1 - 1.6 ppm (figure 3b). This difference between coastal sites is associated with the distinct pollutants emissions between North and South China, which will be discussed further in the section 3.2. Meanwhile, except the pollution episode on 8 April during C1-YS, the concentrations for BC and CO over the sea are less than 4 $\mu g \cdot m^{-3}$ and 1 ppm, respectively. The different concentration ranges between coastal sites and sea areas can be related with the distance to the continental source. The episode in Yellow Sea on 8 April also occurs at Changdao Island from 7 to 8 April (shown in the dashed rectangle in figure 3a and 3b), indicating a regional pollution episode over these areas. The peak concentrations for BC or CO are almost the same, but the peak time in Yellow Sea is delayed almost one day than that at Changdao Island, which could be considered as the transport time between the island and Yellow Sea during the regional pollution.

As illustrated in figure 3, the concentrations of BC and CO fluctuate consistently over the eastern coast of China, which indicates that they are from the same source. Apparently, the consistence during CD, C1 and WL is much better than that during C2. In particular, BC and CO at Wenling site show the best agreement during the period from 22 to 28 November, suggesting the significant impact of the primary emission on the site. The reasons for the above variability will be discussed in the next two sections.

3.2 ΔBC/ΔCO variability and comparison with other studies in East China

Figure 4 shows the relationship between BC and CO for all campaigns. The data points for Yellow Sea in the first cruise (C1-YS) are all overlapped with those for Changdao Island (figure 4a), which is similar with those between East China Sea in the second cruise (C2-ES) and Wenling (figure 4b). It indicates that both C1-YS and CD (or C2-ES and WL) are influenced by the same air mass. However, the data represented by the dashed oval in figure 4b are apart from most of the

data for Wenling campaign. These data correspond to those on 19 November (dashed rectangle in figure 2c) when CO mixing ratio was highest during the campaign and BC mass concentration was relatively low. In the campaign document, a heavy precipitation was recorded in the midnight of 18 November. This is agreed with the different removal mechanism that the precipitation can much easier remove aged BC without affecting CO (Hertel et al., 1995;Girach et al., 2014). So the data

5 impacted by the precipitation are excluded in regressing the ΔBC/ΔCO slope for Wenling. There are not outlier data points for other campaigns, indicating that the effect of the precipitation on BC concentration is negligible. Thus, the loss of BC is expected to be minor due to the absence of precipitation for other campaigns.

The ΔBC/ΔCO ratios at coastal sites are compared with those in other studies in East China (figure 5a) to find out the possible reasons for the different ratios among continental sites. The studies which simultaneously measure BC and CO are

10 centered in the megacities such as Beijing, Shanghai, and Guangzhou (Han et al., 2009;Zhou et al., 2009;Andreae et al., 2008), while there are still rare studies in the north China Plain that emit the most amounts of BC, or the ΔBC/ΔCO ratio is not given in the publication although BC and CO are measured (Sun et al., 2013). Since the continental sites are close to source regions, it is speculated that the ΔBC/ΔCO ratios are determined by the primary emission more than by the atmospheric processing.

15 The strong and positive correlation between BC and CO is attributed to the common sources such as vehicular emissions (Badarinath et al., 2007). In the vehicular emissions, CO is primarily emitted from gasoline vehicles while BC emissions are dominated by diesel vehicles (Han et al., 2009). In a previous study (Zhou et al., 2009), the difference in ΔBC/ΔCO ratios between Beijing and Shanghai has been attributable to the higher percentage of diesel vehicles in Shanghai. As shown in figure 5a, the ΔBC/ΔCO ratios in Beijing and Changdao Island in North China are less than those in Nanjing, Shanghai,

20 Wenling, and Guangzhou in South China, hinting distinct fuel structrues in North and South China. To prove it, the ΔBC/ΔCO at different sites are compared with the ratios of the diesel consumption to the gasoline consumption in each province/city and they show considerable correlation (figure 5b), which confirms that BC and CO are mainly from vehicular emissions. However, the consumption ratio for Changdao Island in Shandong province is lower deviated to the regression line for other sites. The reason is that Changdao Island is a rural site with little vehicle emission, and it is influenced by

25 Beijing and its surrounding regions during winter Asian monsoon when the predominant wind is from northwest (figure 2a). The ratio at Changdao Island is thus less than that in Beijing.

Although the ΔBC/ΔCO ratios and consumption ratios have a good correlation ($R^2 = 0.63$), the consumption ratios can not fully explain the variability of ΔBC/ΔCO ratios. In one aspect, the diesel and gasoline consumption for vehicle is only a part of total fuel consumption. In another aspect, BC and CO are not only controlled by emission from the local province/city, but

30 also by emission transported from other areas on a regional scale. Moreover, other sources such as biomass burning can also contribute to BC and CO, and change the ΔBC/ΔCO ratio.

3.3 BC aging during transport

The variability in the ΔBC/ΔCO ratio can result from the spatial variation of BC and CO source/sink strength (Badarinath et al., 2007). Since most of BC emission sources are centered in East China (figure 1), the variability in the ΔBC/ΔCO ratio depends on emission sources before BC leaves the continent, as indicated by the comparison in the section 3.2 which

5   elucidates the different fuel structures between North and South China. When BC transports to the marine boundary layer, the variability in the ΔBC/ΔCO ratio is only associated with BC aging and removal, given the insignificant anthropogenic sources in the marine. Therefore, the ratios between continental sites and the cruise measurement may be the ideal comparison to reflect the aging extent of BC.

Owing to the aging and removal of BC and the longer atmospheric lifetime of CO, the slopes, i.e. ΔBC/ΔCO ratios and

10   correlation coefficients will decrease together from upwind to downwind areas. The ΔBC/ΔCO ratios for Changdao, C1-YS (excluding the episode data) and C1-ES are 4.58, 3.49, and 1.84 $\mu g \cdot m^{-3} \cdot ppm^{-1}$ respectively, showing a descent trend from north to south over the eastern coast of China (figure 4c). It is consistent with the predominant northwestern wind during the winter monsoon (figure 2a and 2b). Meanwhile, the correlation coefficients reduce from 0.68 to 0.28. So the slope and correlation coefficient determined from the linear regression are possible indicators of the aging and deposition of BC during

15   the transport. It can be evidenced by the pollution episode in Yellow Sea during the first cruise, where BC and CO has a slope of 3.30 $\mu g \cdot m^{-3} \cdot ppm^{-1}$ and a correlation coefficient of 0.68. Though the slope is smaller than that at Changdao Island (4.58 $\mu g \cdot m^{-3} \cdot ppm^{-1}$), they have the same correlation coefficient.

Under the influence of the summer monsoon (figure 2c), East China Sea is located in the downwind of Wenling. The ΔBC/ΔCO ratios for Changdao Island (4.58 $\mu g \cdot m^{-3} \cdot ppm^{-1}$) and C2-ES (4.84 $\mu g \cdot m^{-3} \cdot ppm^{-1}$) are similar, but the ΔBC/ΔCO

20   ratio for Wenling (9.15 $\mu g \cdot m^{-3} \cdot ppm^{-1}$) is two times more than those at CD and C2-ES, which means that the source region for C2-ES is in South China other than in North China. So, the campaigns of C2-ES and WL can be considered as a transport process, though these two campaigns are not simultaneously conducted. The ΔBC/ΔCO ratios and correlation coefficient for C2-ES and WL during the summer monsoon also show a descent trend, as the same as those for CD, C1-YS, and C1-ES during the winter monsoon (figure 4c). Therefore, the decreasing slope and correlation coefficient indicate the more aging

25   and easier removal of BC after outflow from the source regions.

The BC average concentration for C1-ES (0.94 $\mu g \cdot m^{-3}$) during the winter monsoon is only a little higher than that for C2-ES (0.77 $\mu g \cdot m^{-3}$) during the summer monsoon. However, the ΔBC/ΔCO ratio in C1-ES is 8/20 time less than that in Changdao Island, and the ratio in C2-ES is nearly 11/20 time less than that in Wenling, indicating more aging of BC in East China Sea during the winter monsoon. Due to the more extent of aging, BC during the winter monsoon could be more hygroscopic and

30   result in more significant radiative effect (Moffet and Prather, 2009;Bond and Bergstrom, 2006).

4 Conclusions

The atmospheric campaigns including two coastal sites and two cruises were conducted in 2011 to characterize the outflow of primary emission over the eastern coast of China. Due to a large amount of continental pollutant emissions, there were considerable loadings of the primary pollutants in the coast and the sea areas in East China under the influence of the Asian
5 monsoon.

The slope, i.e. ΔBC/ΔCO ratio regressed from the relationship between BC and CO is informative after correcting BC and CO background concentration (Wang et al., 2015). The comparison between the coastal sites of Changdao Island and Wenling and other studies reveals that the fuel structures are different between North and South China. The ΔBC/ΔCO ratios are well associated with the ratios of diesel consumption to gasoline consumption, which may primarily be resulted from the
10 vehicular emission.

The comparison in ΔBC/ΔCO ratios between the coastal site and the sea area reflect the aging and deposition of BC. During the simultaneous measurement of Changdao Island and the first cruise, the ΔBC/ΔCO ratio and the correlation coefficient decrease with time and distance from the source under the influence of the winter monsoon. The ΔBC/ΔCO ratio and the correlation coefficient also show a decreasing trend from Wenling to East China Sea. Therefore, the ΔBC/ΔCO ratio and the
15 correlation coefficient are possible indicators for BC aging and removal after outflow from the source regions.

The authors declare that they have no conflict of interest.

Acknowledgements

This work was supported by National Basic Research Program of China (973 Program) (2013CB228503), National Natural Science Foundation of China (91544214, 41421064) and China Ministry of Environmental Protection's Special Funds for
20 Scientific Research on Public Welfare (201009002). We thank the CAPTAIN team from Peking University, Peking University Shenzhen Graduate School, and Zhejiang Province Environmental Monitoring Center for their help and support for this research.

References

Andreae, M. O., Schmid, O., Yang, H., Chand, D., Yu, J. Z., Zeng, L. M., and Zhang, Y. H.: Optical properties and chemical
25 composition of the atmospheric aerosol in urban Guangzhou, China, Atmos Environ, 42, 6335-6350, 10.1016/j.atmosenv.2008.01.030, 2008.
Badarinath, K. V. S., Latha, K. M., Chand, T. R. K., Reddy, R. R., Gopal, K. R., Reddy, L. S. S., Narasimhulu, K., and Kumar, K. R.: Black carbon aerosols and gaseous pollutants in an urban area in North India during a fog period, Atmos Res, 85, 209-216, Doi 10.1016/J.Atmosres.2006.12.007, 2007.
30 Bond, T., Doherty, S., Fahey, D., Forster, P., Berntsen, T., DeAngelo, B., Flanner, M., Ghan, S., Kärcher, B., and Koch, D.: Bounding the role of black carbon in the climate system: a scientific assessment, Journal of Geophysical Research: Atmospheres, 2013.

Bond, T. C., Streets, D. G., Yarber, K. F., Nelson, S. M., Woo, J.-H., and Klimont, Z.: A technology-based global inventory of black and organic carbon emissions from combustion, Journal of Geophysical Research: Atmospheres, 109, D14203, 10.1029/2003JD003697, 2004.

Bond, T. C., and Bergstrom, R. W.: Light absorption by carbonaceous particles: An investigative review, Aerosol Sci Tech,
5   40, 27-67, 10.1080/02786820500421521, 2006.

De Gouw, J., and Jimenez, J. L.: Organic Aerosols in the Earth's Atmosphere, Environ Sci Technol, 43, 7614-7618, 10.1021/es9006004, 2009.

Feng, J. L., Guo, Z. G., Chan, C. K., and Fang, M.: Properties of organic matter in PM2.5 at Changdao Island, China - A rural site in the transport path of the Asian continental outflow, Atmos Environ, 41, 1924-1935,
10   10.1016/j.atmosenv.2006.10.064, 2007.

Girach, I. A., Nair, V. S., Babu, S. S., and Nair, P. R.: Black carbon and carbon monoxide over Bay of Bengal during W_ICARB: Source characteristics, Atmos Environ, 94, 508-517, Doi 10.1016/J.Atmosenv.2014.05.054, 2014.

Guo, Q., Hu, M., Guo, S., Wu, Z., Hu, W., Peng, J., Hu, W., Wu, Y., Yuan, B., Zhang, Q., and Song, Y.: The identification of source regions of black carbon at a receptor site off the eastern coast of China, Atmos Environ, 100, 78-84,
15   http://dx.doi.org/10.1016/j.atmosenv.2014.10.053, 2015.

Guo, S., Hu, M., Lin, Y., Gomez-Hernandez, M., Zamora, M. L., Peng, J. F., Collins, D. R., and Zhang, R. Y.: OH-Initiated Oxidation of m-Xylene on Black Carbon Aging, Environ Sci Technol, 50, 8605-8612, 2016.

Han, S., Kondo, Y., Oshima, N., Takegawa, N., Miyazaki, Y., Hu, M., Lin, P., Deng, Z., Zhao, Y., Sugimoto, N., and Wu, Y.: Temporal variations of elemental carbon in Beijing, J Geophys Res-Atmos, 114, Artn D23202
20   Doi 10.1029/2009jd012027, 2009.

Hertel, O., Christensen, J., Runge, E. H., Asman, W. A. H., Berkowicz, R., Hovmand, M. F., and Hov, O.: Development and Testing of a New Variable Scale Air-Pollution Model - Acdep, Atmos Environ, 29, 1267-1290, Doi 10.1016/1352-2310(95)00067-9, 1995.

Hitzenberger, R., Petzold, A., Bauer, H., Ctyroky, P., Pouresmaeil, P., Laskus, L., and Puxbaum, H.: Intercomparison of
25   thermal and optical measurement methods for elemental carbon and black carbon at an urban location, Environ Sci Technol, 40, 6377-6383, 2006.

Hu, W. W., Hu, M., Yuan, B., Jimenez, J. L., Tang, Q., Peng, J. F., Hu, W., Shao, M., Wang, M., Zeng, L. M., Wu, Y. S., Gong, Z. H., Huang, X. F., and He, L. Y.: Insights on organic aerosol aging and the influence of coal combustion at a regional receptor site of central eastern China, Atmos. Chem. Phys., 13, 10095-10112, 10.5194/acp-13-10095-2013, 2013.

30   Lee, Y. C., Lam, Y. F., Kuhlmann, G., Wenig, M. O., Chan, K. L., Hartl, A., and Ning, Z.: An integrated approach to identify the biomass burning sources contributing to black carbon episodes in Hong Kong, Atmos Environ, 80, 478-487, 10.1016/j.atmosenv.2013.08.030, 2013.

McMeeking, G. R., Hamburger, T., Liu, D., Flynn, M., Morgan, W. T., Northway, M., Highwood, E. J., Krejci, R., Allan, J. D., Minikin, A., and Coe, H.: Black carbon measurements in the boundary layer over western and northern Europe, Atmos
35   Chem Phys, 10, 9393-9414, 10.5194/acp-10-9393-2010, 2010.

Moffet, R. C., and Prather, K. A.: In-situ measurements of the mixing state and optical properties of soot with implications for radiative forcing estimates, Proceedings of the National Academy of Sciences of the United States of America, 106, 11872-11877, 10.1073/pnas.0900040106, 2009.

Nair, V. S., Moorthy, K. K., Alappattu, D. P., Kunhikrishnan, P. K., George, S., Nair, P. R., Babu, S. S., Abish, B., Satheesh,
40   S. K., Tripathi, S. N., Niranjan, K., Madhavan, B. L., Srikant, V., Dutt, C. B. S., Badarinath, K. V. S., and Reddy, R. R.: Wintertime aerosol characteristics over the Indo-Gangetic Plain (IGP): Impacts of local boundary layer processes and long-range transport, J Geophys Res-Atmos, 112, 2007.

Pan, X. L., Kanaya, Y., Wang, Z. F., Liu, Y., Pochanart, P., Akimoto, H., Sun, Y. L., Dong, H. B., Li, J., Irie, H., and Takigawa, M.: Correlation of black carbon aerosol and carbon monoxide in the high-altitude environment of Mt. Huang in
45   Eastern China, Atmos Chem Phys, 11, 9735-9747, Doi 10.5194/Acp-11-9735-2011, 2011.

Peltier, R. E., Hecobian, A. H., Weber, R. J., Stohl, A., Atlas, E. L., Riemer, D. D., Blake, D. R., Apel, E., Campos, T., and Karl, T.: Investigating the sources and atmospheric processing of fine particles from Asia and the Northwestern United States measured during INTEX B, Atmos Chem Phys, 8, 1835-1853, 2008.

Peng, J. F., Hu, M., Guo, S., Du, Z. F., Zheng, J., Shang, D. J., Zamora, M. L., Zeng, L. M., Shao, M., Wu, Y. S., Zheng, J.,
50   Wang, Y., Glen, C. R., Collins, D. R., Molina, M. J., and Zhang, R. Y.: Markedly enhanced absorption and direct radiative

forcing of black carbon under polluted urban environments, Proceedings of the National Academy of Sciences of the United States of America, 113, 4266-4271, 2016.

Schnaiter, M., Linke, C., Mohler, O., Naumann, K. H., Saathoff, H., Wagner, R., Schurath, U., and Wehner, B.: Absorption amplification of black carbon internally mixed with secondary organic aerosol, J Geophys Res-Atmos, 110, 2005.

5   Spackman, J. R., Schwarz, J. P., Gao, R. S., Watts, L. A., Thomson, D. S., Fahey, D. W., Holloway, J. S., de Gouw, J. A., Trainer, M., and Ryerson, T. B.: Empirical correlations between black carbon aerosol and carbon monoxide in the lower and middle troposphere, Geophys Res Lett, 35, Artn L19816
Doi 10.1029/2008gl035237, 2008.

Sun, Y. W., Zhou, X. H., Wai, K. M., Yuan, Q., Xu, Z., Zhou, S. Z., Qi, Q., and Wang, W. X.: Simultaneous measurement of
10 particulate and gaseous pollutants in an urban city in North China Plain during the heating period: Implication of source contribution, Atmos Res, 134, 24-34, 10.1016/j.atmosres.2013.07.011, 2013.

Wang, Q. Y., Liu, S. X., Zhou, Y. Q., Cao, J. J., Han, Y. M., Ni, H. Y., Zhang, N. N., and Huang, R. J.: Characteristics of Black Carbon Aerosol during the Chinese Lunar Year and Weekdays in Xi'an, China, Atmosphere-Basel, 6, 195-208, 10.3390/atmos6020195, 2015.

15 Wang, Y. X., Wang, X., Kondo, Y., Kajino, M., Munger, J. W., and Hao, J. M.: Black carbon and its correlation with trace gases at a rural site in Beijing: Top-down constraints from ambient measurements on bottom-up emissions, J Geophys Res-Atmos, 116, Artn D24304
10.1029/2011jd016575, 2011.

Yuan, B., Hu, W. W., Shao, M., Wang, M., Chen, W. T., Lu, S. H., Zeng, L. M., and Hu, M.: VOC emissions, evolutions
20 and contributions to SOA formation at a receptor site in eastern China, Atmos. Chem. Phys., 13, 8815-8832, 10.5194/acp-13-8815-2013, 2013.

Zhou, X., Gao, J., Wang, T., Wu, W., and Wang, W.: Measurement of black carbon aerosols near two Chinese megacities and the implications for improving emission inventories, Atmos Environ, 43, 3918-3924,
http://dx.doi.org/10.1016/j.atmosenv.2009.04.062, 2009.

25
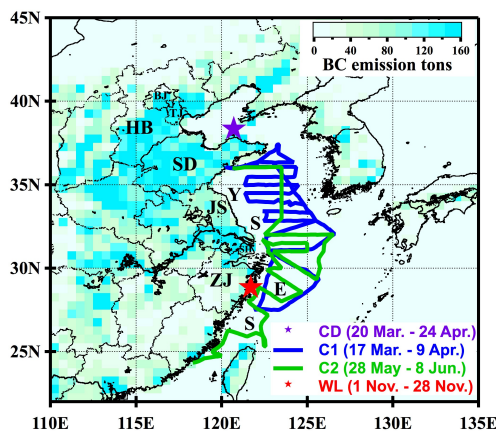
Figure 1. The coastal sites, cruise tracks and their observation periods for the campaigns conducted in 2011. Deep purple star is the coastal site of Changdao Island (CD), and red star is the coastal one of Wenling (WL). Blue line is the track of the first cruise (C1) and green line is the track of the second cruise.The yearly mean anthropogenic emission of BC is also colored on the map

(MEIC, http://www.meicmodel.org). The abbreviation for provinces/cities: BJ - Beijing, TJ - Tianjin, HB - Hebei, SD - Shandong, JS - Jiangsu, SH - Shanghai, ZJ - Zhejiang, YS - Yellow Sea, ES - East China Sea.
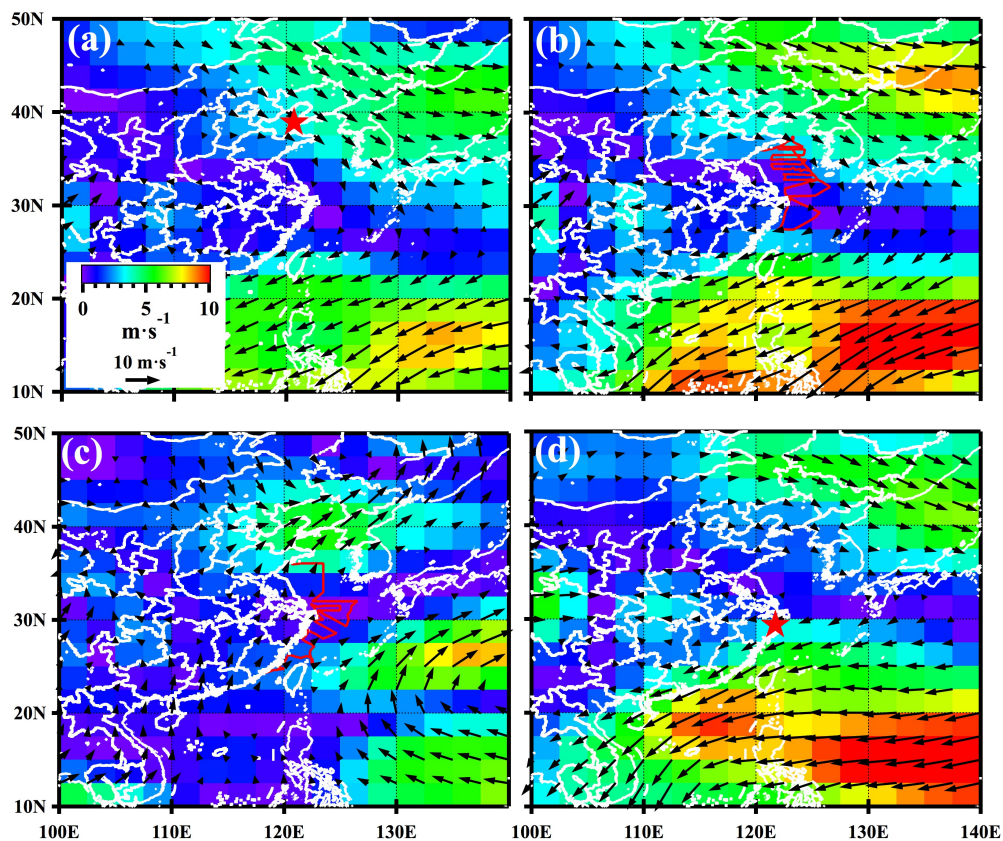
5   Figure 2. The synoptic wind flow patterns at 925 hPa averaged over Changdao Island (a, the red star), the first cruise (b, the red line), the second cruise (c, the red line), and Wenling (d, the red star) campaign periods as shown in Figure 1. The arrow length and the color show the wind speed, while the arrowhead indicates the wind direction.
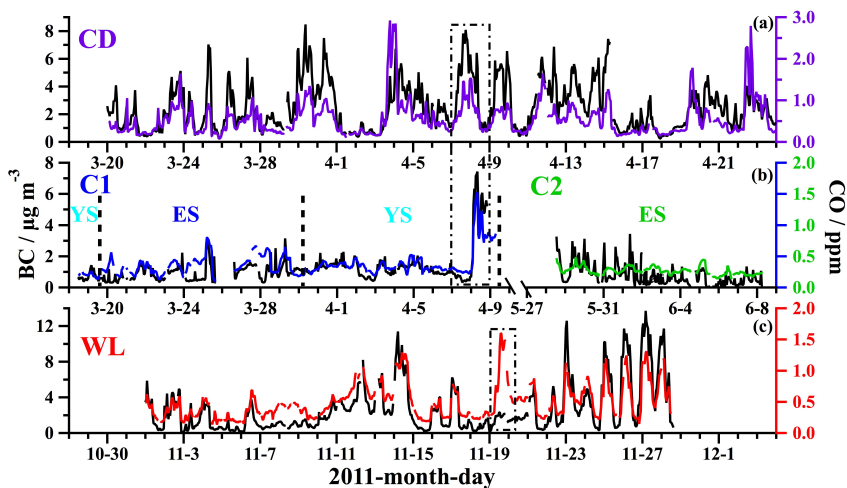
Figure 3. The time series of BC and CO during the campaigns of Changdao Island (a), two cruises (b), and Wenling (c).
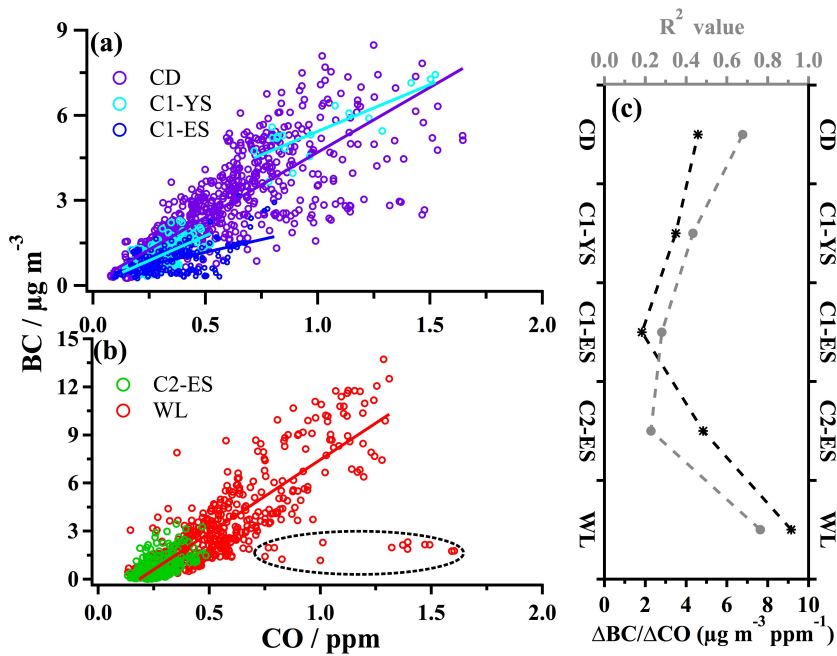
Figure 4. Scatter plots of BC vs. CO (a, b) and their regression slopes and correlation coefficients (c).
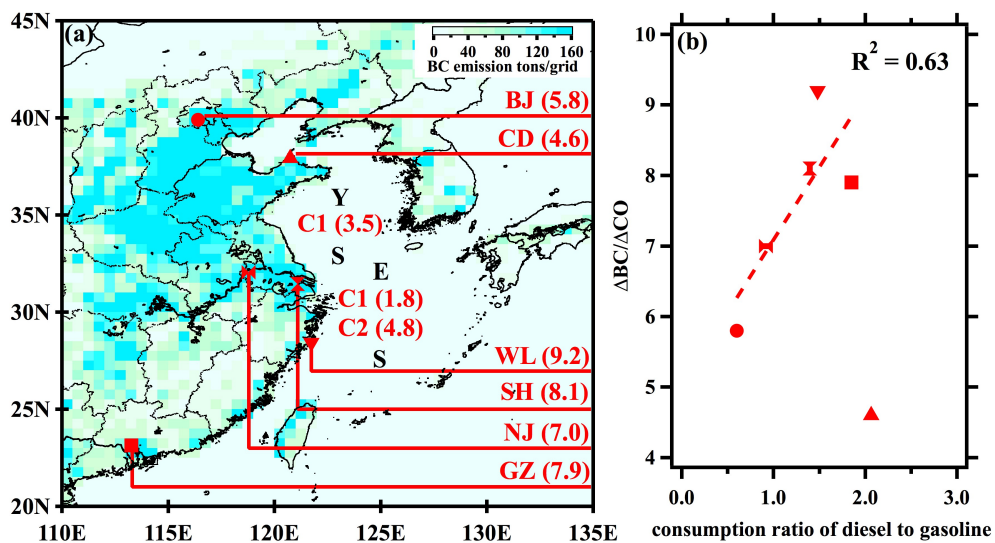
Figure 5. The ΔBC/ΔCO ratios in this study and other studies in East China (a) and their function of the ratios of diesel consumption to gasoline consumption in each province/city (b).